Scheme V

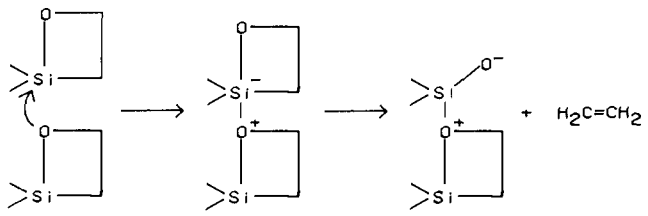

Scheme VI

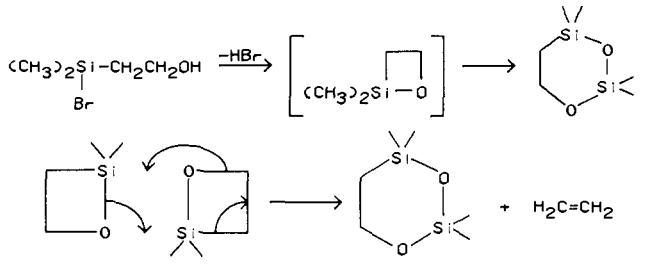

projected electron density about each of the heavy centers (and their associated hydrogens) was performed by using lines of demarkation which approximate the virial surfaces.[32] These integrations appear in Table VI as net charge on each fragment. Of particular interest is the large negative charge on oxygen. The oxygen atom of 1,2-silaoxetane carries well over a full negative charge. Integration of the electron density in cyclodisiloxane gives a net charge on oxygen of −1.58 and −1.65 at 3-21G and 3-21G(*), respectively. The Si–O bond in cyclic systems is clearly quite polar, wiht a substantial negative charge centered on oxygen.

This large charge separation suggests a mechanism for the reaction under study (Scheme V). The oxygen of one silaoxetane molecule can act as a nucleophile toward the silicon of another silaoxetane molecule. This supermolecule can then extrude the alkene, leaving a zwitterion which is capable of forming the silanone oligomers. This mechanism has the benefit of never forming isolated silanone but rather produces directly the oligomers of silanone, a much more enegetically feasible route. Barton[8] has suggested a similar mechanism to explain the reaction of 2-(dimethylsilyl)ethanol with bromine to give 2,2,4,4-tetramethyl-2,4-disila-1,3-dioxane (Scheme VI). Here two silaoxetane molecules combine directly to yield the alkene and the closed form of the zwitterion intermediate proposed above.

(32) McDowell, R. S.; Grier, D. L.; Streitwieser, A., Jr. *Comput. Chem.*, in press.

Conclusion

The Si–O bond in cyclic systems is highly polar, with oxygen carrying greater than a full negative charge. This large negative charge coupled with the strong lone-pair repulsions between the oxygens and slight Si–Si attraction accounts for the unusual structure of cyclodisiloxane.

The reaction of silenes with ketones to give alkenes and siloxanes is driven by the great strength of the many Si–O bonds formed in producing the cyclosiloxanes. Reasonable mechanisms for this reaction must allow for the direct formation of cyclic siloxanes without invoking silanones, since the reaction of silaoxetane to silanone and alkene is strongly endothermic. Silaoxetane has not been isolated due to the large exothermicity involved in proceeding from silaoxetane to alkenes and siloxanes. However, the reverse reaction may allow for the detection of a silaoxetane.

Acknowledgment. This work was supported in part by AFOSR Grant 82-0114. The VAX 11/750 computer system used for the calculations was purchased in part with NSF equipment Grant CHE-82-14313.

Registry No. 5, 71814-15-8; formaldehyde, 50-00-0; silene, 51067-84-6; silanone, 22755-01-7; ethylene, 74-85-1; cyclodisiloxane, 34392-10-4.

Stability of the Reaction Coordinate in the Unimolecular Reaction of Thioformaldehyde

Akitomo Tachibana,*† Iwao Okazaki,† Masahiko Koizumi, Kenzi Hori,‡ and Tokio Yamabe†

Contribution from the Department of Hydrocarbon Chemistry, Faculty of Engineering, Kyoto University, Kyoto 606, Japan. *Received July 13, 1984*

Abstract: A dynamical aspect of the unimolecular photodissociation reaction of thioformaldehyde is analyzed and compared to the photodissociation reaction of formaldehyde. A characteristic feature of the out-of-plane vibrational mode, which is orthogonal to the reaction coordinate, is revealed. The force constant of the out-of-plane vibrational mode is considerably softened in the neighborhood of the transition state. The electronic structure of this softening mechanism is clarified. This softening may destabilize the reaction coordinate and broaden the area accessible for the reactive flux to pass through the transition state. This may affect the dynamics of the photodissociation reaction considerably.

I. Introduction

One of the principal subjects of recent theoretical chemistry is the study of the dynamical processes in chemical reaction systems. Particularly in photochemical reactions, dynamical processes involving rovibronic energy transfers have recently received much attention.[1,2] In this field of research, the Born–Oppenheimer adiabatic approximation of electronic motion plays a fundamental role, and certain characteristic features of chemical reaction paths are analyzed by using this approximation. Fukui's intrinsic reaction coordinate (IRC) approach provides a firm theoretical basis for the study of the chemical reaction paths.[3] The

†Division of Molecular Engineering, Graduate School of Engineering, Kyoto University, Kyoto 606, Japan.

‡Present address: Department of Chemistry, Faculty of Liberal Arts, Yamaguchi University, Yamaguchi 753, Japan.

(1) (a) Jaffe, R. L.; Morokuma, K. *J. Chem. Phys.* **1976**, *64*, 4881. (b) Heller, D. F.; Elert, M. L.; Gelbart, W. M. *Ibid.* **1978**, *69*, 4061. (c) Kemper, M. J. H.; van Dijk, J. M. F.; Buck, H. M. *J. Am. Chem. Soc.* **1978**, *100*, 7841. (d) Goddard, J. D.; Schaefer, H. F., III. *J. Chem. Phys.* **1979**, *70*, 5117. (e) Goddard, J. D.; Yamaguchi, Y.; Schaefer, H. F., III. *Ibid.* **1981**, *75*, 3459. (f) Ho, P.; Bamford, D. J.; Buss, R. J.; Lee, Y. T.; Moore, C. B. *Ibid.* **1982**, *76*, 3630. (g) Moore, C. B.; *Annu. Rev. Phys. Chem.* **1983**, *34*, 525. (h) Dupuis, M.; Lester, W. A., Jr.; Lengsfield, B. H., III; Liu, B. *J. Chem. Phys.* **1983**, *79*, 6167.

(2) (a) Goddard, J. D.; Clouthier, D. J. *J. Chem. Phys.* **1982**, *76*, 5039. (b) Clouthier, D. J.; Ramsay, D. A. *Annu. Rev. Phys. Chem.* **1983**, *34*, 31. (c) Pope, S. A.; Hillier, I. H.; Guest, M. F. *J. Chem. Soc., Chem. Commun.* **1984**, *623*.

0002-7863/85/1507-1190$01.50/0

IRC traces the most characteristic regions on the adiabatic potential energy surface and connects the stable equilibrium points of the reactants to the products passing through the unstable transition state (TS). The dynamical energy transfers in a chemical reaction are analyzed with respect to nuclear motion along the IRC and vibrational motions which are orthogonal to the IRC. In this respect, the general theory of the stability of the reaction coordinate has been developed, where rovibronic energy transfers between nuclear motion along the reaction coordinate and orthogonal degrees of freedom (including electronic motion and the small vibrational motions) are taken into consideration.[4] The potential energy surface U along the reaction coordinate is therefore represented as

$$U(s,\Delta y^\alpha) = U(s) + \tfrac{1}{2}\sum k_{\alpha\alpha}\Delta y^\alpha\Delta y^\alpha + \tfrac{1}{6}\sum k_{\alpha\beta\gamma}\Delta y^\alpha\Delta y^\beta\Delta y^\gamma + \tfrac{1}{24}\sum k_{\alpha\beta\gamma\delta}\Delta y^\alpha\Delta y^\beta\Delta y^\gamma\Delta y^\delta \quad (1)$$

where s, Δy^α, and the k's denote, respectively, the reaction coordinate, the orthogonal vibrational coordinate, and the force constants. Thus, a chemical reaction system can be represented by a single particle immersed in a $3N - 6$ dimensional space accompanied by $3N - 7$ vibrational bosons (N denoting the number of nuclei in the system). The chemical reaction dynamics is characterized by the correlation of the representative particle with the vibrational bosons.[5] Thus, using the IRC approach, we have a theoretically simple picture for studying the characteristic features of the chemical reaction dynamics.

Recent progress in the theory of chemical reaction dynamics has been based on studies of small organic molecules. As one of the simplest organic molecules, formaldehyde has played an important role in this field of research.[1] Two recent topics in formaldehyde chemistry are the unimolecular dissociation reaction

$$H_2CO \rightarrow TS1 \rightarrow H_2 + CO \quad (2)$$

and the unimolecular isomerization reaction

$$H_2CO \rightarrow TS2 \rightarrow HCOH\ (trans) \quad (3)$$

Of particular interest to the dynamical processes of these reactions are the effects due to tunneling[6] and, for the dissociation reaction 2, the mode specificity.[7] Likewise, another simple organic molecule, thioformaldehyde, has received due attention,[2] yet its dynamical processes await further investigation. In this paper, we shall study the unimolecular reaction characteristics of thioformaldehyde in terms of the IRC approach. We shall focus our attention on the unimolecular dissociation reaction

$$H_2CS \rightarrow TS3 \rightarrow H_2 + CS \quad (4)$$

The characteristic features of the stability of the reaction coordinate are analyzed and compared to the corresponding reaction of formaldehyde. The reaction 4 pathway maintains C_s symmetry, and the coupling with the out-of-plane vibrational motion, which is orthogonal to the IRC, shows very interesting behavior as will be discussed later. This behavior is peculiar to the dissociation reaction of H_2CS and was not found for H_2CO.[7] Therefore, we shall also analyze the intramolecular isomerization reaction of thioformaldehyde which possesses similar out-of-plane nuclear motions

$$H_2CS \rightarrow TS4 \rightarrow HCSH\ (trans) \quad (5)$$

Reaction 5 is considered to be the counterpart of reaction 3 for the isomerization of formaldehyde.

Table I. Activation Energy (E_a) and Heat of Reaction (ΔH) (kcal/mol)

	6-31G**//6-31G**	CID/6-31G**//6-31G**	CID+Q/6-31G**//6-31G**
disso.			
E_a	107.88	102.47	99.95
ΔH	46.63	43.62	46.22
isomer			
E_a	96.09	96.08	94.11
ΔH	46.76	52.52	53.42

II. Methods of Calculation

The molecular orbital (MO) calculations were carried out with the GAUSSIAN 80[8] programs by using the restricted Hartree–Fock method[9] with a 6-31g**[10a] basis set. Geometry optimization of the reactants, products, and TS's was performed by using the energy gradient method.[11] The electron correlation energy was estimated by double-substituted configuration interaction (CID).[12] The Davidson correction[13] was added to allow for unlinked cluster quadruple correction (QC). The MO contour maps, configuration analysis,[14] and energy decomposition[15] were performed. The vibrational analysis and IRC were calculated with the HONDO[16] program by using the same basis set. The second derivatives of the potential energy surface, required for the vibrational analysis of the TS structure, were obtained by numerical differentiation of the analytical energy gradients.[17]

III. Results and Discussion

A. Geometries, Potential Profiles, and Reaction Path Analysis. The optimized geometries of reactants, products, and TS's of reactions 4 and 5 and net atomic charges are shown in Figure 1. The TS's were identified as the structure of a saddle point on the potential energy surface by vibrational analysis. For the reactions of H_2CO, TS1 and TS2 have C_s symmetry, and, therefore, the major dynamical processes of reactions 2 and 3 are characterized by the C_s symmetry. Likewise, for the reactions of H_2CS, the dominant dynamical processes of reactions 4 and 5 may be characterized by the C_s symmetry. However, TS4 for the transisomerization reaction 5 of H_2CS doesn't have symmetry higher than C_1 because the migrating hydrogen is located out of plane. This special character of the present reaction system H_2CS and its resulting characteristic dynamical aspect will be discussed in terms of the stability of the reaction coordinate in section IIIC. This characteristic feature of the isomerization reaction system of H_2CS as compared to H_2CO is also found for the dissociation reaction 4, which will be clarified in the following discussions.

The potential energy profile for the dissociation reaction 4 and the transisomerization reaction 5 is depicted in Figure 2 a and b, respectively. The abscissa represents the corresponding IRC: the origin corresponds to the TS, the negative side corresponds to the reactant region, and the positive side corresponds to the product region. Activation energies and heats of reaction are summarized in Table I. The activation energies for H_2CS show that the transisomerization reaction 5 is more likely to occur than

(3) (a) Fukui, K. *J. Phys. Chem.* **1970**, *74*, 4161. (b) Fukui, K.; Kato, S.; Fujimoto, H. *J. Am. Chem. Soc.* **1975**, *97*, 1. (c) Ishida, K.; Morokuma, K.; Komornicki, A. *J. Chem. Phys.* **1977**, *66*, 2153.
(4) Tachibana, A.; Fukui, K. *Theor. Chim. Acta* **1979**, *51*, 275.
(5) (a) Tachibana, A.; Fukui, K. *Theor. Chim. Acta* **1978**, *49*, 321. (b) Tachibana, A. *Ibid.* **1979**, *51*, 189. (c) Hofacker, G. L. *Z. Naturforsch., A* **1963**, *18A*, 607. (d) Hofacker, G. L. *Int. J. Quantum Chem.* **1969**, *3S*, 33. (e) Brickmann, J. *Z. Naturforsch. A* **1973**, *28A*, 1759. (f) Russegger, P.; Brickmann, J. *J. Chem. Phys.* **1975**, *62*, 1086.
(6) Miller, W. H. *J. Am. Chem. Soc.* **1979**, *101*, 6810.
(7) (a) Yamashita, K.; Yamabe, T.; Fukui, K. *Chem. Phys. Lett.* **1981**, *84*, 123. (b) Miller, W. H.; *J. Am. Chem. Soc.* **1983**, *105*, 216.
(8) Pople, J. A.; et al. *QCPE* **1981**, *13*, 406.
(9) Roothaan, C. C. J. *Rev. Mod. Phys.* **1951**, *23*, 69.
(10) (a) Francl, M. M.; Pietro, W. J.; Herhe, W. J.; Binkley, J. S.; Gordon, M. S.; DeFrees, D. J.; Pople, J. A. *J. Chem. Phys.* **1982**, *77*, 3654. (b) Ditchfield, R.; Hehre, W. J.; Pople, J. A. *J. Chem. Phys.* **1971**, *54*, 724.
(11) Pulay, P. In "Modern Theoretical Chemistry"; Schaefer, H. F., III, Ed.; Plenum Press: New York, 1977; Vol. 4, Chapter 4.
(12) Seeger, R.; Krishnan, R.; Pople, J. A. *J. Chem. Phys.* **1978**, *68*, 2519.
(13) (a) Langhoff, S. R.; Davidson, E. R. *Int. J. Quantum Chem. 8*, **1974**, 61. (b) Davidson, E. R.; Silver, D. W. *Chem. Phys. Lett.* **1978**, *52*, 403.
(14) (a) Murrell, J. N.; Randic, M.; Williams, D. R. *Proc. R. Soc. London, Ser. A* **1965**, *A284*, 566. (b) Baba, H.; Suzuki, S.; Takemura, T. *J. Chem. Phys.* **1969**, *50*, 2078. (c) Fujimoto, H.; Kato, S.; Yamabe, S.; Fukui, K. *Ibid.* **1974**, *60*, 572. (d) Nagase, S.; Fueno, T. *Theor. Chim. Acta* **1974**, *35*, 217. (e) Nagase, S.; Fueno, T. *Ibid.* **1976**, *41*, 59.
(15) Kitaura, K.; Morokuma, K. *Int. J. Quantum Chem.* **1976**, *10*, 325. We used the IMSPACK program (Morokuma, K.; Kato, S.; Kitaura, K.; Ohmine, I.; Sakai, S.; Obara, S. IMS Computer Center Library Program No. 0372, 1980.
(16) Dupuis, M.; King, H. F. *J. Chem. Phys.* **1978**, *68*, 3998.
(17) (a) McIver, W. J.; Komornicki, A. *Chem. Phys. Lett.* **1971**, *10*, 303. (b) Komornicki, A.; Ishida, K.; Morokuma, K.; Ditchfield, R.; Conrad, M. *Ibid.* **1977**, *45*, 595.

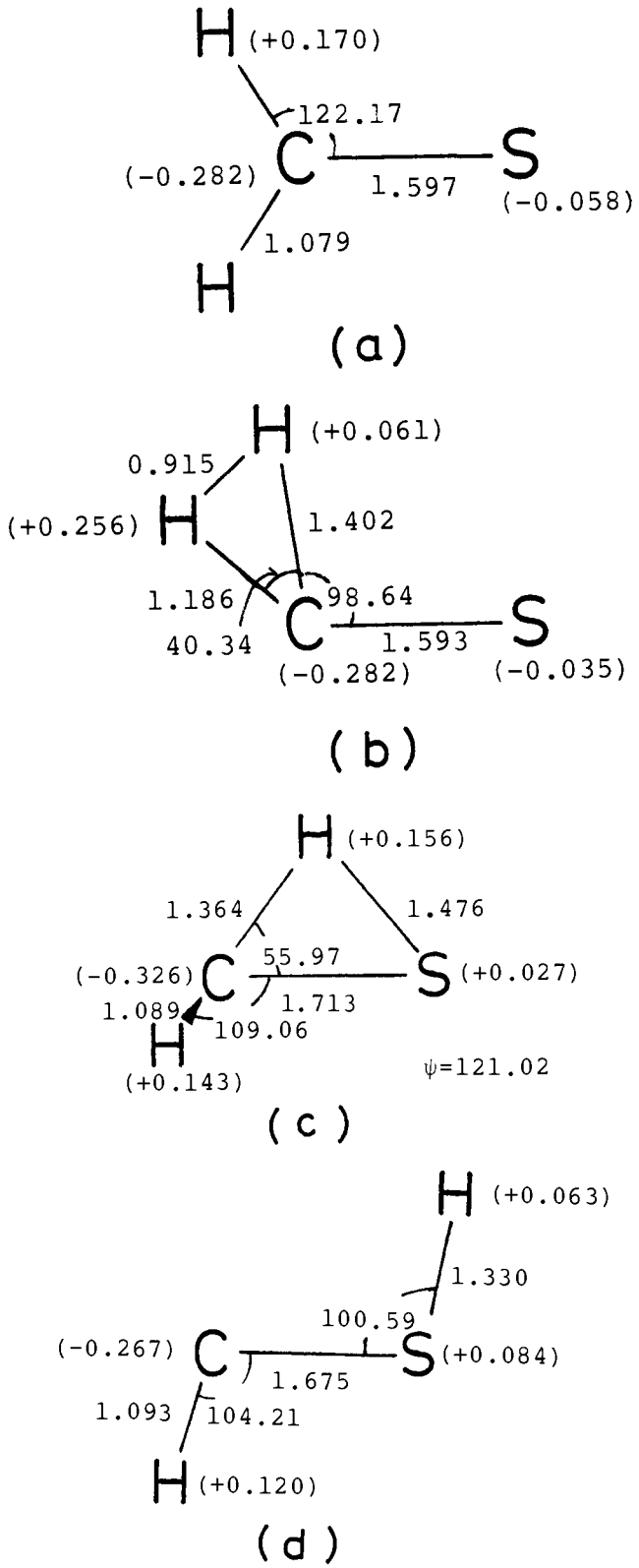

Figure 1. Optimized geometries of (a) reactant, (b) TS of dissociation, (c) TS of isomerization, and (d) trans isomer of H_2CS. Net atomic charges are shown in the parentheses. Bond lengths and angles are given in angstroms and degrees, respectively, ψ is the dihedral angle ∠HCSH.

the dissociation reaction 4; this is also true for H_2CO.[1e] Figure 3 a and b shows the changing geometry along the IRC for the dissociation reaction of H_2CO and H_2CS, respectively. Let us analyze first the dissociation reaction of H_2CS. As shown in Figure 3b, when moving along the reaction coordinate toward the product, the change of distance between the carbon atom and each leaving hydrogen of H_2CS is of similar magnitude, and, accordingly, the

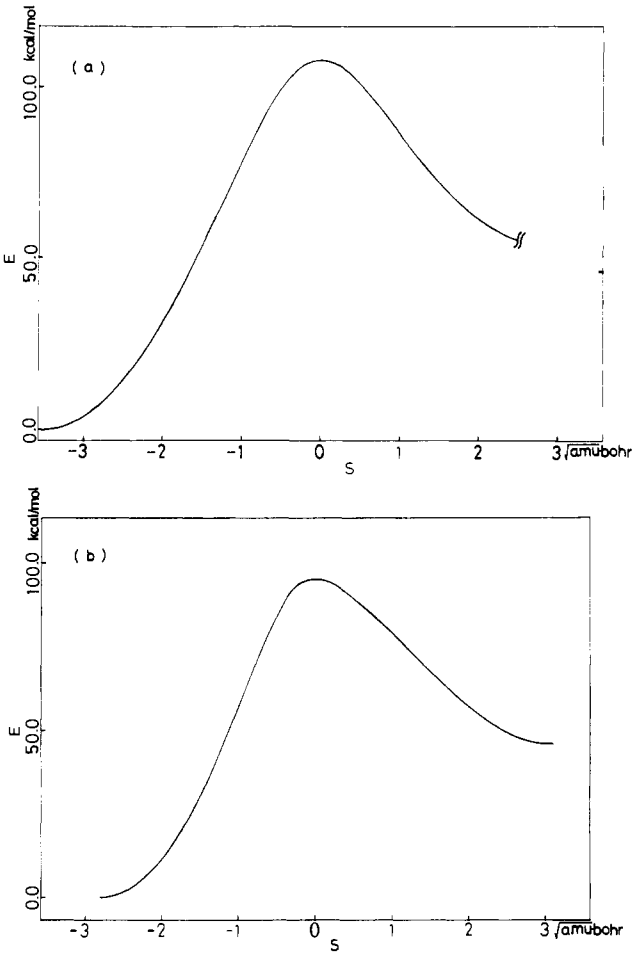

Figure 2. Potential energy profile along the IRC for the (a) dissociation and (b) isomerization reactions.

formation of the hydrogen molecule progresses smoothly. The hydrogen molecule is nearly produced at TS3. As shown in Figure 1, in the dissociation reaction of H_2CS (eq 4), the H–H distance (0.915 Å) of the TS3 is closer to that of the product H_2 (0.733 Å) than that of the reactant H_2CS (1.826 Å)—TS3 is closer to the product than to the reactant. The net charges on the atoms in TS3 show that the charge distribution on CS is not very different from the reactant but that on H–H polarization is substantial. On the other hand, in the dissociation reaction of H_2CO, as shown in Figure 3 a, the change in distance between the carbon atom and each leaving hydrogen is not in step with each other. Indeed, at TS1, the formation of the hydrogen molecule is not near completion. The H–H distance (1.320 Å) in TS1 shows an intermediate value between the reactant (1.837 Å) and the product (0.730 Å). Interestingly, at TS1, the distance between the leaving hydrogen atoms is nearly equal to the equilibrium distance of H_2^- ($^2\Sigma^+_u$).[18] This is the major difference between the reaction coordinate for the dissociation reactions 2 and 4. The changes of the other geometrical parameters are similar to each other. In particular, it should be noted that the CO and CS bond lengths are almost unchanged throughout the course of the reaction.

B. Electronic Structure of the Transition State. In this subsection, TS3 for the dissociation reaction of H_2CS (eq 4) is divided into two subsystems, H_2 and CS, and the interaction between them is analyzed in order to clarify the electronic structure of the transition state.

As described in section IIIA, both of the subsystems CS and H_2 nearly attain their equilibrium structures at TS3. Figure 4 shows the energy levels and the occupation numbers for the HOMO and LUMO of H_2 and CS: the HOMO is π_{CS} and

(18) (a) Herzenberg, A.; Kwok, K. L.; Mandl, F. *Proc. Phys. Soc., London* **1964**, *84*, 477. (b) Kolos, W.; Wolniewicz, L. *J. Chem. Phys.* **1965**, *43*, 2429.

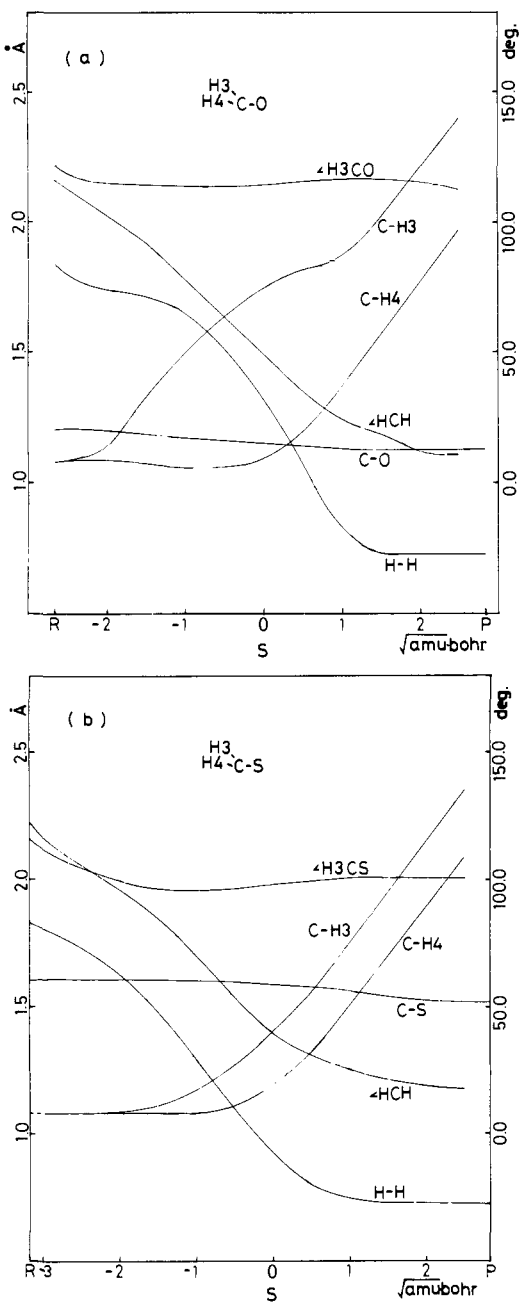

Figure 3. Changes of geometries along the IRC for the dissociation reaction of (a) H_2CO and (b) H_2CS. R and P denote the reactant and product, respectively. The basis set used for H_2CO calculation is 4-31G.[10b]

LUMO is π^*_{CS}, both of which are doubly degenerate. The occupation numbers in Figure 4 show that the π_{CS} orbitals do not strongly contribute to the active electronic interaction processes. The HOMO–LUMO energy split of the CS subsystem is 13.89 eV with the n_{CS} orbital lying slightly (0.63 eV) below the HOMO. The HOMO–LUMO energy split of the H_2 subsystem is 20.12 eV. Characteristic electronic processes, such as charge transfer (CT) or polarization (PL), which are observed in these subsystems, are analyzed in terms of configuration analysis.[14] The results of configuration analysis are represented as

$$\Psi_{H_2CS} = 0.377\Psi_0 + 0.140\Psi_{n-\sigma^*} - 0.141\Psi_{n-\pi^*} + 0.314\Psi_{\sigma-\pi^*} - 0.052\Psi_{\sigma-\sigma^*} + 0.108\Psi_{2(\sigma-\pi^*)} - 0.082\ \Psi_{\sigma,n-\pi^*} + 0.097\Psi_{n,\sigma-\pi^*,\sigma^*} \quad (6)$$

where Ψ_0 stands for the adiabatically interacting configuration, Ψ_{i-j} indicates the configuration in which one electron is transferred from MO i to MO j, and $\Psi_{2(i-j)}$ and $\Psi_{i,j-k,l}$ indicate configurations for two-electron transfers.

Table II. Scheme of Energy Decomposition

tot energy	E°
electrostatic energy	E_{ES}
exchange energy	E_{EX}
$CT(\sigma \rightarrow \pi^*_{CX}) + PL(n_{CX} \rightarrow \pi^*_{CX}) + EX$	E_{FCTPLX}
$CT(n_{CX} \rightarrow \sigma^*) + PL(\sigma \rightarrow \sigma^*) + EX$	E_{BCTPLX}

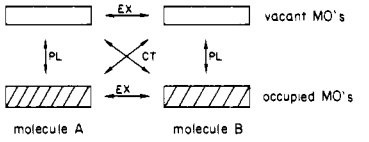

$$\Delta E^\circ = E^\circ_A + E^\circ_B - E^\circ$$
$$\Delta E_{ES} = E_{ES} - E^\circ$$
$$\Delta E_{EX} = E_{EX} - E_{ES}$$
$$\Delta E_{FCTPLX} = E_{FCTPLX} - E_{EX}$$
$$\Delta E_{BCTPLX} = E_{BCTPLX} - E_{EX}$$
$$\Delta E^\circ = \Delta E_{ES} + \Delta E_{EX} + \Delta E_{FCTPLX} + \Delta E_{BCTPLX} + \Delta E_{MIX}$$

Table III. Results of the Energy Decomposition (au)

ΔE°	−0.074 76
ΔE_{ES}	−0.242 11
ΔE_{EX}	0.529 05
ΔE_{FCTPLX}	−0.218 99
ΔE_{BCTPLX}	−0.090 71
ΔE_{MIX}	−0.052 00

The contribution for CT (σ–π^*) which is given as 0.314 is the largest and that for CT (n–σ^*) which is given as 0.140 is also large. These contributions are enhanced if double-excitation configurations are included. As is well-known, the influence of CT depnds mostly on the overlap of the MO's. To examine this MO distribution maps of the π^*_{CS} and n_{CS} orbitals at the TS3 geometry of CS are shown in Figure 5 a and b, respectively. It should be noted that the distribution of the frontier orbitals in the vicinity of S is remarkable. This contribution of S will facilitate an overlap of the frontier orbitals of CS with those of H_2 in TS3 and, thus, may play an important role in the CT interaction between the two subsystems. Likewise, the influence of PL reflects the difference between the energy levels which tak part in the virtual excitation process. In this case, the HOMO–LUMO energy split is 6.23 eV smaller in CS than in H_2. This may explain the fact that the PL(n–π^*) contribution which is given as 0.141 is greater than that for PL(σ–σ^*) which is given as 0.052 from the configuration analysis.

The contributions of the interaction energies were studed in terms of the scheme of energy decomposition.[15] First, the interaction energies were decomposed into four interaction energy terms: the electrostatic energy (E_{ES}), the exchange repulsion energy (E_{EX}), the polarization energy (E_{PL}), and the charge-transfer energy (E_{CT}). Second, by rearranging these terms, the total interaction energy (ΔE_0) was decomposed into the five components as shown in Table II. The character of the interaction, CTPLX, is not merely the additive contributions of the CT, PL, and EX components, but is a composite of these terms. In other words, the important electronic process of CT will induce the virtual excitation process of PL, and this combined effect is denoted as CTPLX. The residues are denoted as MIX. The results of energy decomposition are shown in Table III (the negative sign means that the interaction yields stabilization). It follows that the stabilization due to CT(σ–π^*), which is given as ΔE_{FCTPLX} = −0.21899, is greater than the stabilization due to back CT(n–σ^*), which is given as ΔE_{BCTPLX} = −0.09071. This is reasonable considering the results of the configuration analysis.

Thus, the characteristic electronic processes which play an important role at the TS3 geometry in the dissociation reaction 4 have been analyzed. The interactions between the subsystems H_2 and CS are very strong, with the major contributions of CT and PL being emphasized.

C. Stability of the Reaction Coordinate. In this subsection, a dynamical aspect of the dissociation reaction 4 is analyzed. Figure 6 shows the frequency changes of the vibrational modes

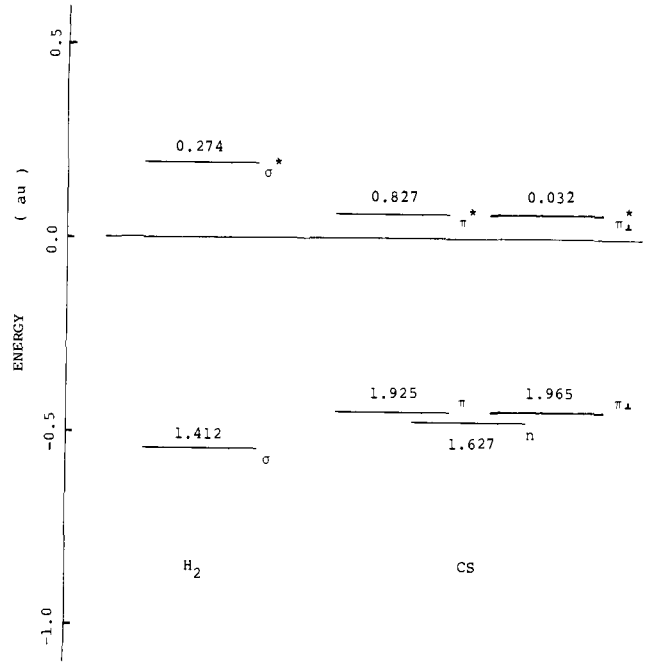

Figure 4. Energy levels and the occupation numbers for the HOMO and LUMO subsystems of H_2CS.

Table IV. Coefficient of Configuration Analysis

	π^*	$\pi^*_\perp$	σ^*
0.3			
n	0.0665	0.0101	0.0707
π	0.0186	0.0020	0.0032
$\pi_\perp$	0.0004	0.0148	0.0023
σ	0.1594	0.0060	0.0639
0.2			
n	0.0672	0.0068	0.0716
π	0.0189	0.0013	0.0035
$\pi_\perp$	0.0003	0.0149	0.0016
σ	0.1614	0.0040	0.0636
0.1			
n	0.0676	0.0035	0.0722
π	0.0191	0.0007	0.0036
$\pi_\perp$	0.0002	0.0149	0.0008
σ	0.1627	0.0020	0.0634
0.0			
n	0.0677	0.0	0.0723
π	0.0192	0.0	0.0037
$\pi_\perp$	0.0	0.0150	0.0
σ	0.1631	0.0	0.0633

orthogonal to the reaction path, as a function of the reaction coordinate s, from the reactant to TS3. Reaction 4 maintains C_s symmetry from the reactant to the product through TS3. The out-of-plane vibrational mode has an imaginary frequency around $s = -0.8$. This indicates that the potential energy decreases in a direction orthogonal to the IRC around $s = -0.8$. For the reaction of H_2CO, the out-of-plane vibrational mode has a minimum around $s = -0.8$, but is amplitude remains positive all along the IRC.[7] Figure 7 shows the potential energy profile for the direction orthogonal to the IRC at $s = -0.8$. The displacement is linear according to the displacement vector for the out-of-plane vibrational mode. The potential energy decreases of this out-of-plane nuclear motion as is expected from the imaginary frequency. The electronic process of this interesting dynamical behavior of the IRC was analyzed further. The orbital occupation numbers for the subsystems as a function of the out-of-plane motion orthogonal to the IRC at $s = -0.8$ are depicted in Figure 8. For increasing deformation, the occupation of σ decreases and σ^* increases. Likewise, with increasing deformation, the occupation decreases for n_{CS} and $\pi_{CS\perp}$ and increase for $\pi^*_{CS\perp}$, where

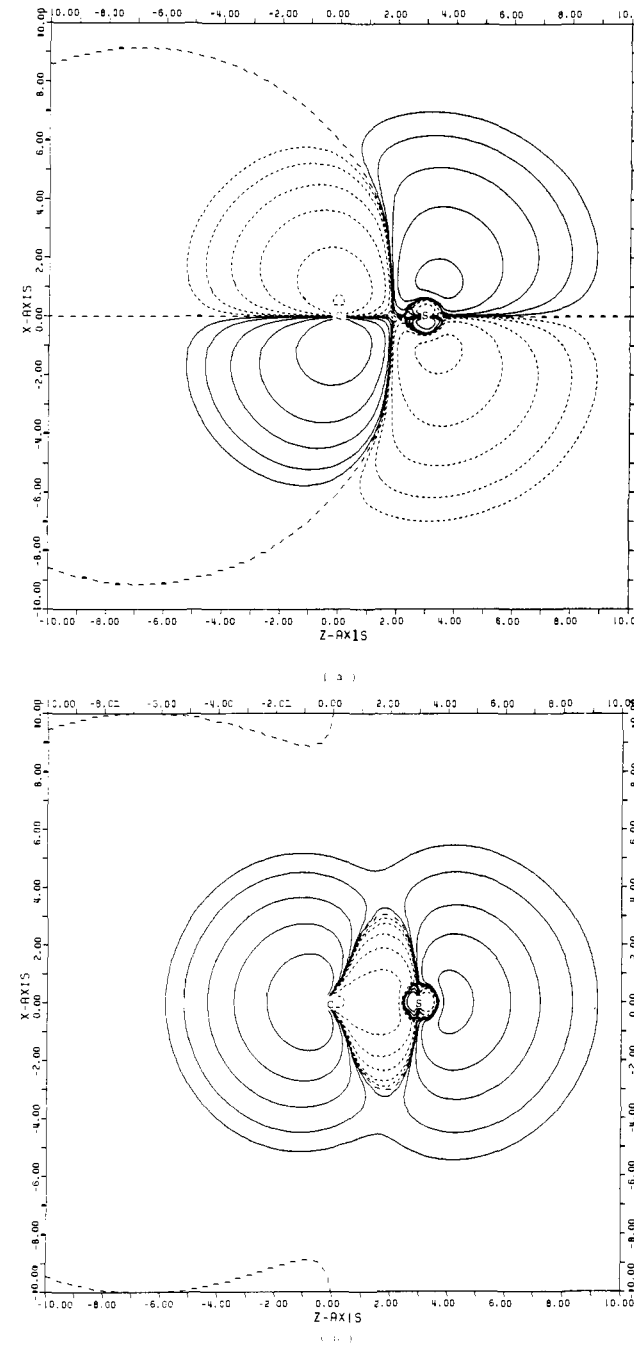

Figure 5. Contour maps of (a) π^*_{CS} and (b) n_{CS} of CS at the TS3 bond length.

$\pi_{CS\perp}$ denotes the π orbital of CS whose distribution is out of plane. The novel contributions of the $\pi_\perp$ orbitals are peculiar to this out-of-plane deformation, and the new interactions of CT(σ–$\pi^*_{CS\perp}$) and PL(n–$\pi^*_{CS\perp}$) will play an important role for this deformation. Indeed, the results of configuration analysis, as shown in Table IV, clearly support this interpretation. Thus, the characteristic electronic processes of this interesting dynamical behavior along the IRC are clarified.

This novel out-of-plane force should broaden the region available for dissociation reaction 4 to occur. This is closely connected to the stability of the reaction coordinate. It should be noted that the stability of the reaction coordinate may play an important role in chemical reaction dynamics.[4,19] If the orthogonal vibrational modes were hard, then the fluctuations of nuclear motion along the reaction coordinate would be small. In other words, in order to excite the orthogonal mode, the energy required would be so large that the excitation would not occur easily, while, on the other

(19) Mezey, P. G. *Theor. Chim. Acta* **1980**, *54*, 95.

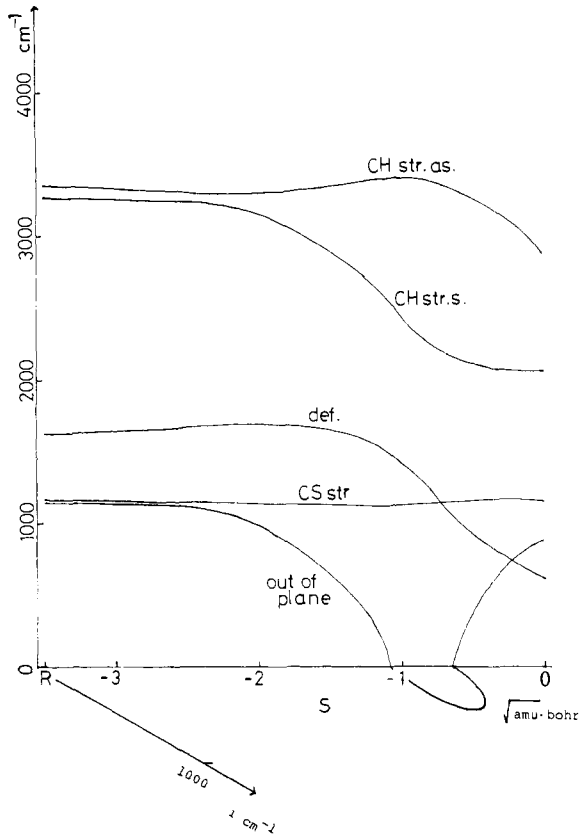

Figure 6. Frequencies of the vibrational modes orthogonal to the IRC, as a function of the reaction coordinate s, from reactant to the TS3. R denotes the reactant.

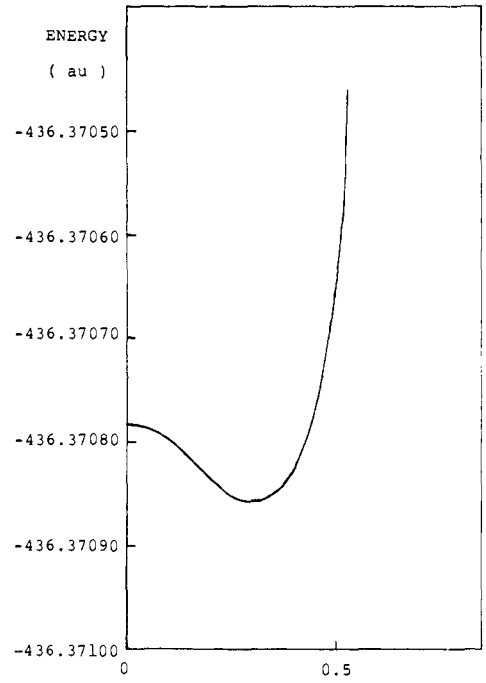

Figure 7. Potential energy profile in the direction orthogonal to the IRC at $s = -0.8$. The scale on the abscissa is the coefficient of non-mass-weighted displacement vector.

hand, if the orthogonal vibrational modes were soft, then the fluctuations of nuclear motion along the reaction coordinate could be large, and then the nuclear motion along the reaction coordinate would become unstable. Thus, little energy would be required to bypass the IRC, the range for the chemical reaction would be broad, and the area accessible for the reactive flux would be enlarged. For this case, the second-order instability is introduced through the CT (σ–$\pi^*_{CS\perp}$) interactions along the out-of-plane

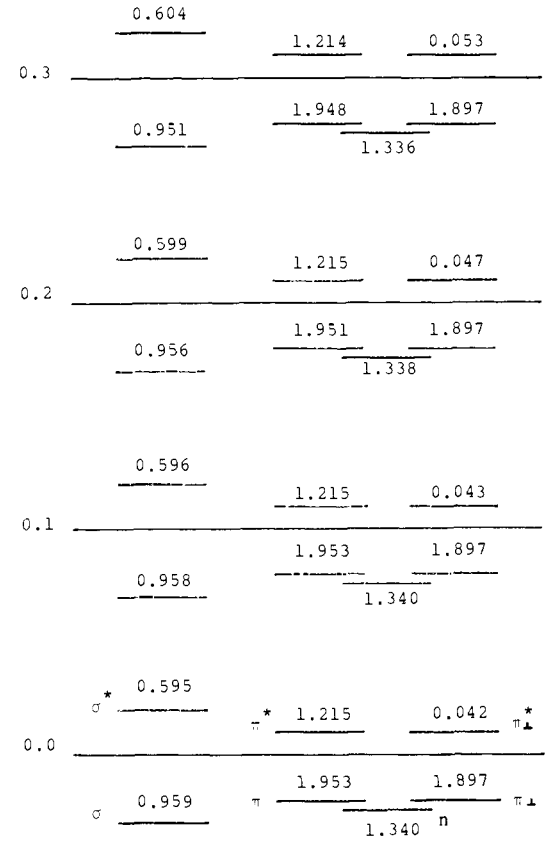

Figure 8. Changes of the occupation numbers as a function of orthogonal deformations at $s = -0.8$. The number of the left-hand side of the figure is the coefficient of non-mass-weighted displacement vector.

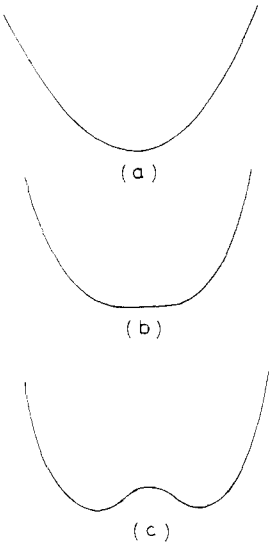

Figure 9. Parabolic potential profile along Δy at each s. (a) $s < -1.1$, (b) $s = -1.1$, (c) $-1.1 < s < -0.7$.

vibrational mode, orthogonal to the reaction coordinate. The potential energy surface along the IRC may be written as

$$U(s,\Delta y) = U(s) + \tfrac{1}{2}k_2(s)\Delta y^2 + \tfrac{1}{24}k_4(s)\Delta y^4$$

$$k_4(s) \geq 0 \qquad (7)$$

where s, Δy, k_2, and k_4 denote the IRC, the out-of-plane vibrational coordinate, the second-order force constant, and the fourth-order anharmonic force constant, respectively. The force constants depend parametrically on s. k_2 may change sign but k_4 is assumed to be positive. For $s < -1.1$, k_2 is positive and we have a parabolic potential profile along Δy at each s, as is shown schematically in Figure 9 a. At $s = -1.1$, k_e becomes 0, and we have the potential

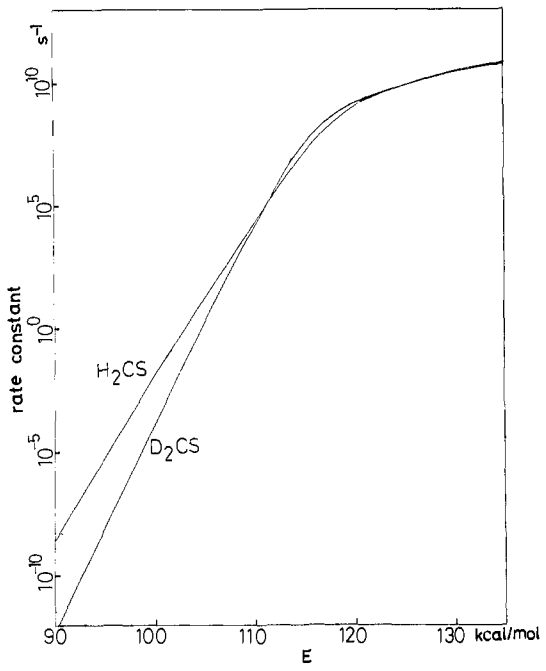

Figure 10. Unimolecular rate constants of the reaction 4 as function of the total energy E.

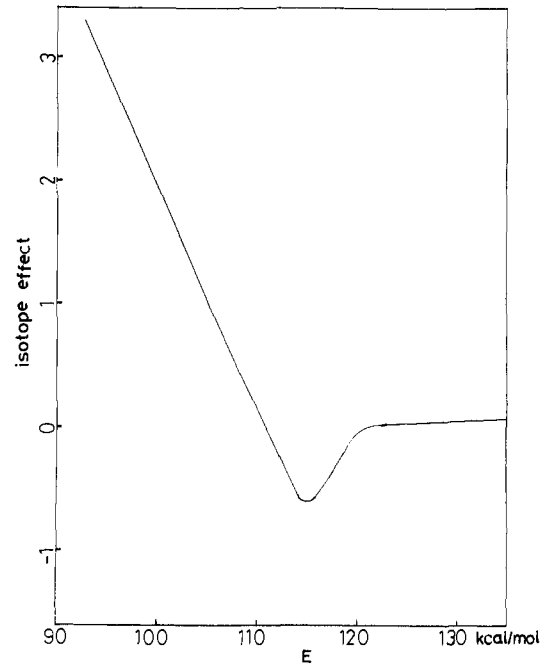

Figure 11. Logarithm of the ratio of the hydrogen rate constant to the deuterium rate constant.

profile of Figure 9b. In the interval $-1.1 < s < -0.7$, k_2 is negative and nuclear motion along the IRC becomes unstable as shown in Figure 9c. The stable equilibrium path disappears when

$$\Delta y_{eq}(s) = \pm(-6k_2(s)/k_4(s))^{1/2} \quad (8)$$

The force constant at this new equilibrium point is given as

$$k_{2,eq}(s) = -2k_2(s) \quad (9)$$

This is twice the unstable force constant and is independent of the fourth-order anharmonic force constant. Along the IRC from $s = -0.7$ to the point of the transition state, $s = 0.0$, the stability of the IRC is recovered; however, the value of k_2 is still small. This shows that the out-of-plane mode can play an important role on the dynamics of the fragmentation reaction—it may have the crucial effect to broaden the chemical reaction path over the transition state and to enhance the tunneling probability of the potential barrier. If the chemical reaction proceeds maintaining C_S symmetry, then the active dynamic contribution of the out-of-plane mode is forbidden. But in the present reaction 4 the out-of-plane mode may have significant effect on the dynamics along the reaction coordinate. Indeed, if the out-of-plane mode is first activated, then the C_s symmetry of the reaction coordinate may be broken dynamically. If it occurs, the contribution of the other reaction 5 which has purely out-of-plane TS and lesser activation energy may become significant in order to treat the whole dynamics of the vibrationally activated H_2CS.

D. Tunneling in the Dissociation Reaction of H_2CS. In this subsection, we shall give a discussion about the effects of tunneling in the transition-state theory of unimolecular reactions. Unimolecular rate constants were obtained, including tunneling corrections to RRKM theory;[6] Figure 10 shows the unimolecular rate constant of reaction 4 as a function of the total energy E. Isotope effects were also calculated. The tunneling is substantial for $E < V$ and is negligible for $E < V_0$, where V and V_0 denote the energy barriers of reaction with and without zero-point energy, respectively. Figure 11 shows the logarithm of the ratio of the hydrogen rate constant to the deuterium rate constant as a function of total energy. There is a minimum point in the vicinity of the classical threshold; this may be the result of differing zero-point energies for H_2CS and D_2CS. This feature has been noted previously by Miller[6] for the dissociation reaction of H_2CO.

It should be noted that the present calculation was based on a one-dimensional model of tunneling along the reaction coordinate. If broadening of the reaction path is taken into account (which is considered substantial for this reaction as discussed in section IIIC), then the reaction rate should be enhanced especially in the lower energy region.

IV. Concluding Remarks

This paper discusses an aspect of the dynamics for the dissociation reaction of H_2CS from the viewpoint of the IRC approach. The intimate relationship between the characteristic out-of-plane electronic processes and the stability of the reaction coordinate is revealed. A brief discussion is also given concerning the reaction rate and how it may be influenced by the stability of the reaction coordinate.

The experiment determining the fluorescence lifetime of the singlet vibrational levels of H_2CS and D_2CS in the $\tilde{A}^1A_2$ state has already been performed,[20] and the out-of-plane mode for the dissociation reaction path on the singlet ground-state surface has been estimated to be important for an accurate analysis of the system dynamics. Thus, the results of these calculations for reaction rates is of interest with regard to the importance of the out-of-plane mode as indicated by experiment. It should be noted that the recent work on the rearrangement and fragmentation of thioformaldehyde[2c] and the most recent work on the molecular dissociation of formaldehyde[1h] indicate the importance of more sophisticated wave function with respect to the electron correlation as well as the basis set quality for the description of the transition-state structure. Therefore, further rigorous treatments of the potential energy surface along the reaction coordinate should be of great help in order to settle the firm foundation of the stability of the reaction coordinate.

Thus, this study of the reaction coordinate dynamics has brought to light an important facets concerning reaction dynamics. It is expected that the success of this approach will encourage similar reaction dynamics studies.

Acknowledgment. This work was supported by a Grant-in-Aid for Scientific Research from the Ministry of Education of Japan, for which we express our gratitude. The numerical calculations were carried out at the Data Processing Center of Kyoto University and the Computer Center of the Institute for Molecular Science (IMS). We also thank Dr. H. Teramae for his assistance with the CI calculation and Dr. K. Yamashita for the use of his vibrational analysis program.

Registry No. Thioformaldehyde, 865-36-1; deuterium, 7782-39-0.

(20) Kawasaki, M.; Kasatani, K.; Sato, H. private communication.